Hindawi
Journal of Nanomaterials
Volume 2020, Article ID 4679061, 14 pages
https://doi.org/10.1155/2020/4679061

*Research Article*

# Voltammetric Determination of Rhodamine B Using a ZIF-67/Reduced Graphene Oxide Modified Electrode

**Huynh Truong Ngo,[1,2] Vo Thang Nguyen,[3] Tran Duc Manh,[3] Tran Thanh Tam Toan,[1] Nguyen Thi Minh Triet,[4] Nguyen Thanh Binh,[5] Nguyen Thi Vuong Hoan,[6] Tran Vinh Thien,[7] and Dinh Quang Khieu[1]**

[1]*University of Sciences, Hue University, 49000, Vietnam*
[2]*TT-Hue Department of Food Safety and Hygiene, 49000, Vietnam*
[3]*University of Education and Science, The University of Da Nang, 50000, Vietnam*
[4]*Ly Thai To High School, 70000, Vietnam*
[5]*Dalat Nuclear Research Institute, 66000, Vietnam*
[6]*Qui nhon University, 55000, Vietnam*
[7]*University of Natural Resource and Environment of Ho Chi Minh City, 70000, Vietnam*

Correspondence should be addressed to Tran Vinh Thien; tvthien@hcmunre.edu.vn
and Dinh Quang Khieu; dqkhieu@hueuni.edu.vn

Received 6 April 2020; Accepted 11 May 2020; Published 3 June 2020

Guest Editor: Yu Liu



In the present article, the synthesis of zeolite imidazolate framework-67/reduced graphene oxide (ZIF-67/rGO) and voltammetric determination of Rhodamine B (RhB) are demonstrated. The obtained materials were characterized by X-ray diffraction, scanning electron microscopy, transmission electron microscopy, X-ray photoelectron spectroscopy, and nitrogen adsorption/desorption isotherms. It was found that the ZIF-67/rGO composite consists of ZIF-67 nano-particles highly dispersed on the rGO matrix and possesses a high specific surface area. Because of the synergistic effect of good conductivity of rGO and high surface area of ZIF-67, the ZIF-67/rGO—modified glassy carbon electrode exhibits good electrochemical behavior toward Rhodamine B (RhB) oxidation. The use of this electrode to quantitate RhB with differential pulse voltammetric method was successful with a broad linear range, from 0.96 to 44.07 $\mu g.L^{-1}$ of RhB and a low limit of detection of 1.79 $\mu g.L^{-1}$. The procedure was able to be applied to quantitatively determine RhB content in several food samples with an exceptional recovery rate (98-103%). The quantitative results highly agreed with that provided by high-performance liquid chromatography, revealing that this material is promising in *in situ* monitoring of other illegal additives in food.

## 1. Introduction

Rhodamine B (RhB), 9-(2-carboxyphenyl)-6-diethylamino-3-xanthenylidene]-diethylammonium chloride), is one of the xanthene dyes and is highly water-soluble. It is the most common synthetic dyes employed as a colorant in textiles, foodstuffs, plastic, leather, and paper [1]. RhB is thought to be a carcinogen and to exhibit developmental toxicity, neurotoxicity, and chronic toxicity towards humans and animals. It has been illegally used to provide the red color in chili powder and sauces as one of the methods of economically motivated adulteration. Thus, due to the health risks arose from RhB consumption, there have been intensive research efforts to develop a simple method for the determination of RhB in different sample matrix. Some methods are available for the determination of RhB such as spectrophotometric determination with micelle-mediated cloud point extraction [2], UV-Vis Spectrophotoscopy following solid phase extraction [3], magnetic solid phase extraction using ionic liquid-coated core–shell magnetic nanoparticles followed by high-performance

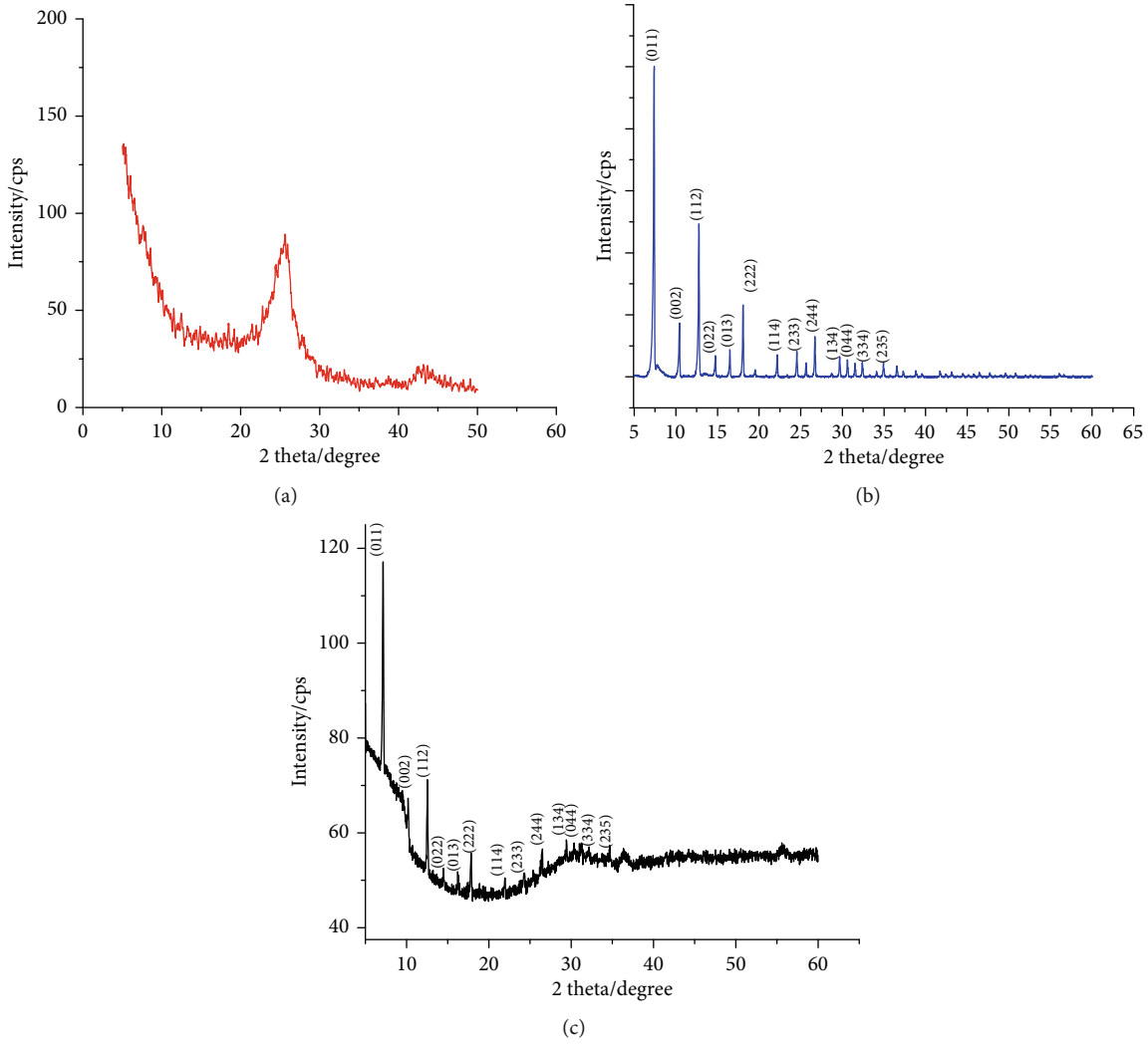


Figure 1: XRD patterns of (a) rGO, (b) ZIF-67, and (c) ZIF-67/rGO.

liquid chromatography [4], and high-pressure liquid chromatography (HPLC) [5, 6]. However, the fact that the operational procedure is complicated, and the cost is high limits the application of these approaches.

The voltammetric approaches have been recognized as the potential methods for the detection of organic and inorganic compounds in trace amount as they offer a simple, low cost, highly selective, and *in situ* operational procedure. The voltammetric method has been employed for the detection of RhB in which it was used to determine RhB in food [7–9]. The development of novel electrodes by modifying them with hybrid organic-inorganic materials provides potential tools in trace analysis of not only RhB but other organic and inorganic substances. Several modified electrodes such as exfoliated graphene-modified electrode [7], silica-pillared zirconium phosphate/nafion composite (SPZP/NAF)-modified electrode [8], betacyclodextrin functionalized nanogold/hollow carbon nanosphere nanohybrid (beta-CD-AuNPs/HCNS)-modified electrode [9], and core-shell-structured Cu@carbon sphere (Cu@CS) nanohybrid-modified electrode have been developed to determine RhB content in different samples by voltammetric methods. Zeolitic imidazolate frameworks-67 (ZIF-67), which are constructed from the tetrahedrally coordinated divalent cations $Co^{2+}$ linked by the imidazolate ligands, are typical ZIFs with high thermal and chemical stability, as well as tunable zeotype topologies. ZIF-67 have been applied in gas storages and adsorption catalyst [10, 11] but has been rarely employed in electrochemistry due to its poor electronic conductivity. Reduced graphene oxide (rGO), an oxidized form of graphene, has attracted great interest in the nanoelectronics and electrochemical industry because it has exhibited outstanding properties such as superior electrical conductivity, high surface area, and chemically stable behaviors. The combination of desirable properties of ZIF-67 and rGO expects a versatile electrode modifier. To our knowledge, few works in the literature have studied the voltammetric determination of Rhodamine B using ZIF-67/rGO/GCE.

In the present paper, the ZIF-67/rGO was synthesized by the microwave-assisted method. The ZIF-67/rGO modified GCE was obtained by drop-casting ZIF-67/rGO suspension on the electrode surface. The electrochemical behaviors of ZIF-67/rGO/GCE were investigated by means of cyclic and

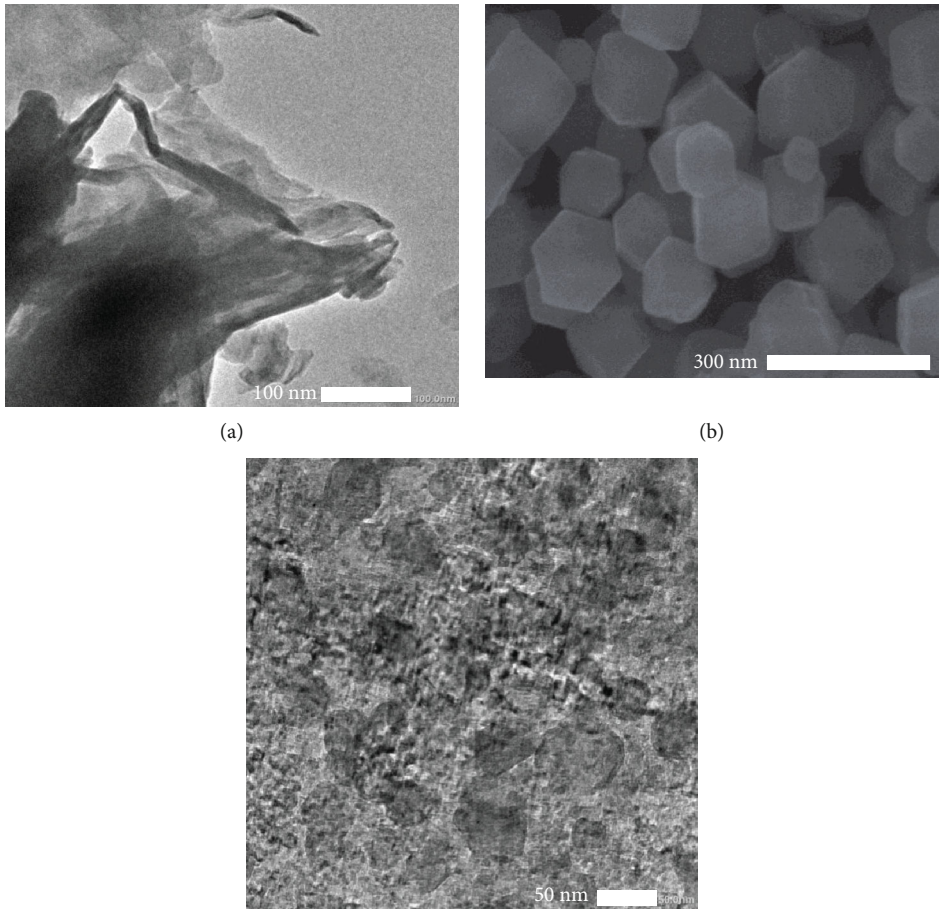


Figure 2: (a) TEM image of rGO. (b) SEM image of ZIF-67. (c) TEM image of ZIF-67/rGO.

differential pulse voltammetry. The modified electrode was employed to determine the RhB in food samples using different pulse voltammetry method, and the results were compared with those from high-performance liquid chromatography.

## 2. Experimental

*2.1. Materials.* Cobalt (II) nitrate hexahydrate ($Co(NO_3)_2{\cdot}6H_2O$, Daejung, Korea) and 2-methylimidazole ($C_4H_6N_2$, Sigma-Aldrich, U.S.A., 99%) were used to prepare ZIF-67. Graphite powder, potassium permanganate ($KMnO_4$), sodium acetate ($NaCH_3COO$), sodium citrate ($Na_3C_6H_5O_7$), acetic acid ($CH_3COOH$, 96%), citric acid ($C_6H_8O_7$), boric acid ($H_3BO_3$), ammonia solution ($NH_4OH$, 25%), and ascorbic acid ($C_8H_6O_6$, 99.7%) were purchased from Merck company (Germany). Sodium nitrate ($NaNO_3$), ethanol ($C_2H_5OH$, 99%), hydroperoxide ($H_2O_2$, 30%), and potassium hydroxide (KOH) were provided by Daejung company (Korea). Britton–Robinson buffer solutions (BR-BS) were prepared from 0.5 M $H_3BO_3$, 0.5 M $H_3PO_4$, and 0.5 M $CH_3COOH$ solutions. The desired pH buffer was adjusted using 1 M KOH or 1 M $H_3PO_4$ solutions.

*2.2. Instrumentation.* The morphologies of ZIF-67, GO and ZIF-67/rGO were observed by scanning electron microscopy (SEM) using SEM JMS–5300LV (Japan) and by transmission electron microscopy (TEM) using JEOL-2100F microscope. Ramma spectra were obtained by XPLORA, HORIBA with laser excitation wavelength of 532 nm. Fourier transformation Infrared (FT-IR) analyses were recorded on a Shimadzu IR Prestige–21 (Japan). X-ray diffraction (XRD) patterns were recorded using D8 Advance—Bruker (Germany) with $CuK_\alpha$ radiation ($\lambda = 0.1514$ nm). X-ray photoelectron spectra (XPS) were collected by using a Shimadzu Kratos AXISULTRA DLD spectrometer (Japan). Voltammetric experiments were undertaken at room temperature using a CPA-HH5 Computerized Polarography Analyser (Vietnam) electrochemical workstation. A three-electrode cell configuration, comprising a glassy-carbon working electrode (GCE) with a diameter of $2.8 \pm 0.1$ mm, the GCE or the modified GCE were used for formatting the modified electrode as a working electrode, an Ag/AgCl/3 M KCl reference electrode, and a platinum wire auxiliary electrode was employed in these experiments.

The Schimadzu 2030 HPLC system was used to analyze Rhodamine B. The chromatographic conditions were as follows: UV detector ($\lambda = 275$ nm), flow rate of 2.0 mL·min$^{-1}$ with the injection volume of 10 $\mu$L, column temperature of $45^\circ C \pm 1^\circ C$. The quantitative analysis was performed with external standardisation by measuring the peak areas on the chromatograms.

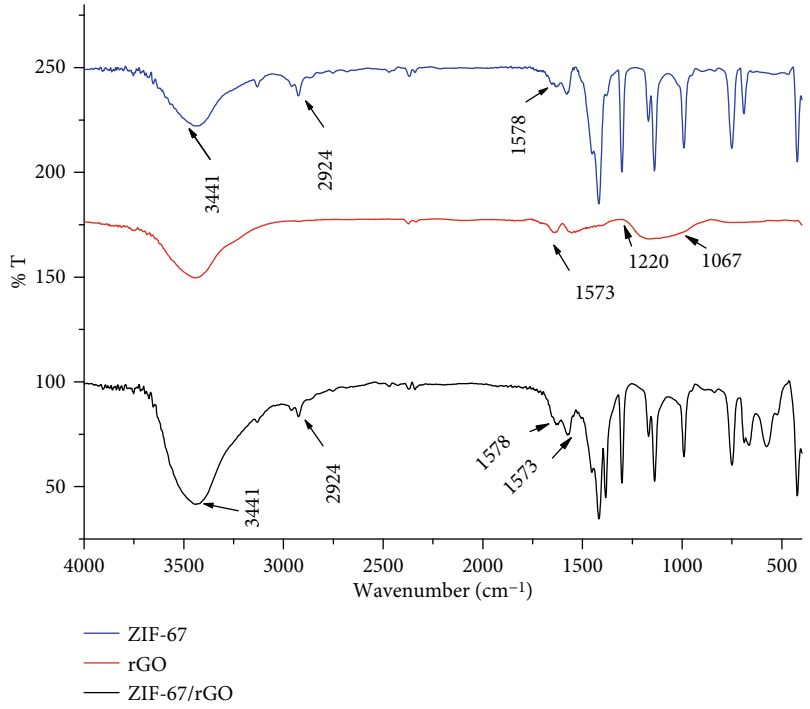


Figure 3: FT-IR spectra of ZIF-67, rGO, and ZIF-67/rGO.

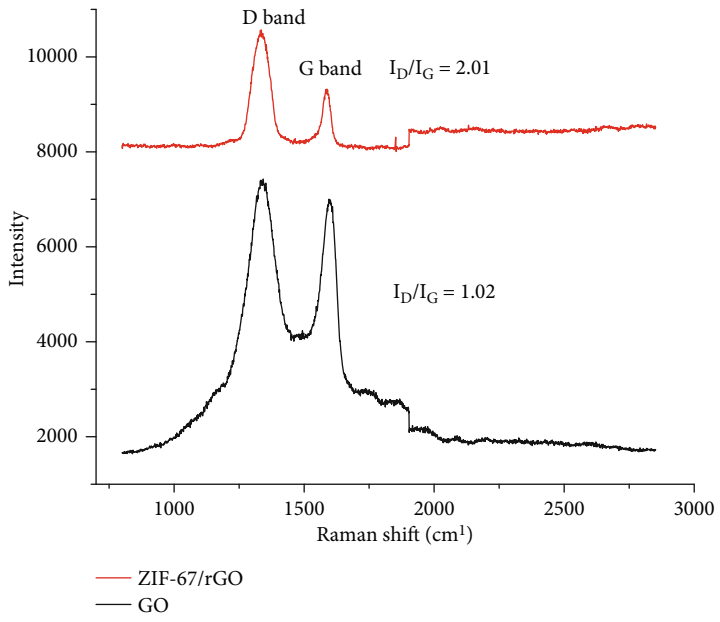


Figure 4: Raman spectra of rGO và ZIF-67/rGO.

### 2.3. Preparation of ZIF-67/rGO

*2.3.1. Preparation of rGO (Reduced Graphene Oxide).* Graphite oxide was generated from graphite powder using the Hummers process [12]. Briefly, 3.0 grams of graphite was added to a mixture containing 120.0 mL concentrated $H_2SO_4$ and 14.0 mL concentrated $H_3PO_4$ solution, followed by a gradual addition of 6.0 g $KMnO_4$ to this suspension under stirring for 72 hours. 6.0 mL of cold $H_2O_2$ (30%) was then added to this suspension under stirring for 10 minutes. The obtained solid was separated by centrifuging and washed with a 1.0 M HCl solution until a clear supernatant was clear. The final solid obtained by centrifuging was washed with distilled water to remove any HCl residue. The yellow-brown solid of graphite oxide was obtained after drying at 65°C for 12 hours and then finely ground. The graphite oxide (0.1 g) was exfoliated by ultrasonication in 100.0 mL of distilled water for 1 h to obtain an aqueous suspension of graphene

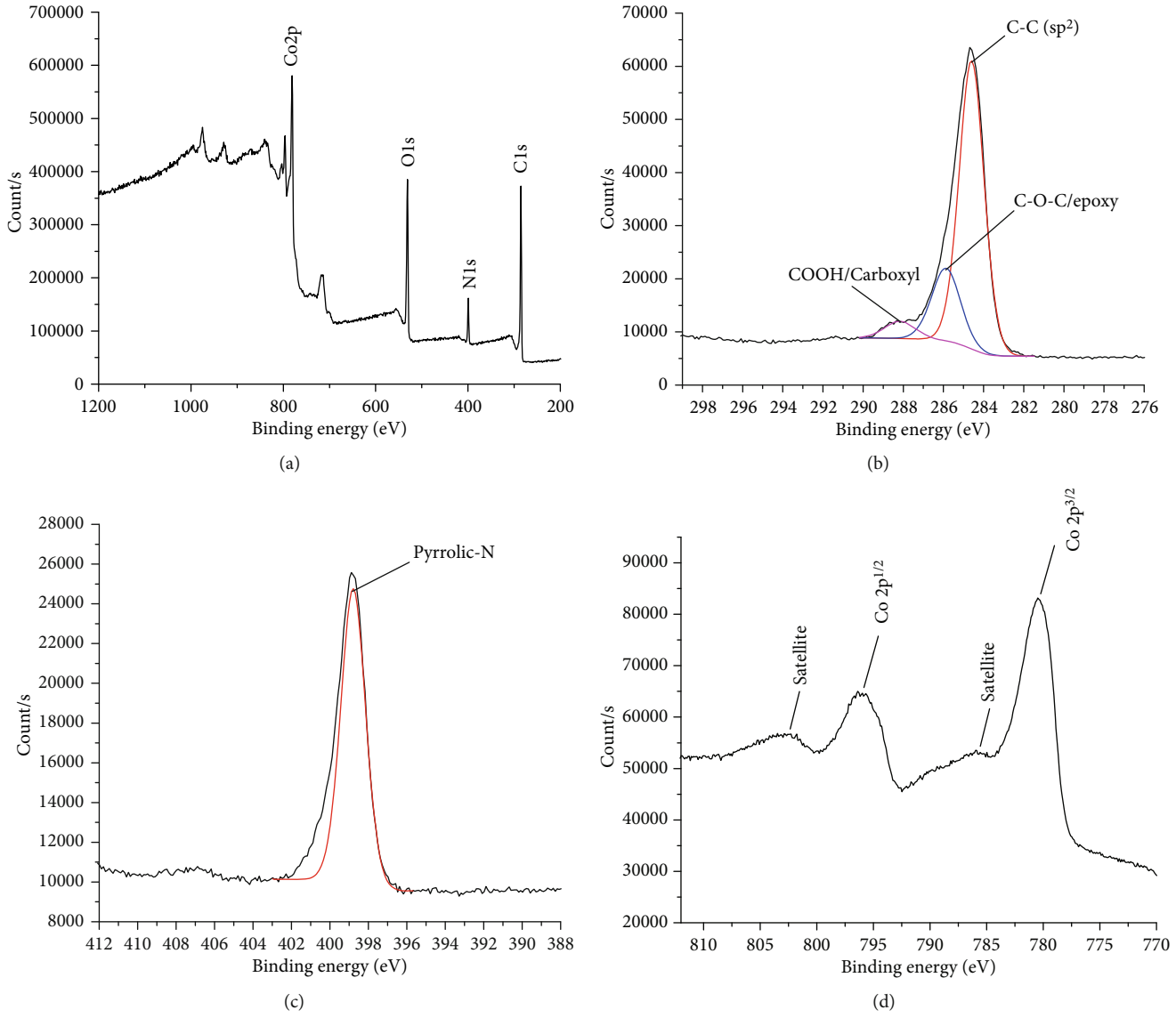


Figure 5: (a) XPS survey spectrum of ZIF67/rGO. (b) XPS C1s spectrum. (c) XPS N1s spectrum. (d) XPS Co2p spectrum.

oxide. Ascorbic acid (0.15 g) was introduced slowly to the graphene oxide suspension, and the mixture was stirred for 8 hours at 50°C to reduced GO. The reduced graphene oxide (rGO) was separated by centrifugation and washed several times with ethanol and dried at 80°C in a vacuum oven for 5 h.

*2.3.2. Preparation of ZIF-67 and ZIF-67/rGO Composite.* A solvent containing a mixture of ethanol: distilled water: DMF (1 : 1 : 1 in w/w) (denoted as solvent A) was prepared. For the synthesis of ZIF-67/rGO, a stable aqueous suspension of rGO (0.025 g of rGO in 50.0 mL of solvent A) was prepared under ultrasonic irradiation for 1 hour. Then, 10.0 mL of 0.1 M cobalt salt in solvent A was added to this suspension and stirred for 3 hours at ambient temperature. Subsequently, 10.0 mL of 0.2 $g.L^{-1}$ 2-methylimidazole solution in solvent A was also introduced under microwave irradiation for 15 minutes. The final product (ZIF-67/rGO composite) was washed several times with ethanol and distilled water and dried at 80°C in a vacuum oven for 5 h.

The ZIF-67 was also synthesized according to the reference [13] for comparison. Briefly, 2-methylimidazole (16.0 mmol) and $Co(NO_3).6H_2O$ (4.0 mmol) were added into 200.0 mL of a mixture of ethanol: distilled water: DMF (1 : 1 : 1 in *w*/*w*). The resulting mixture was treated by the microwave irradiation time for 40 min (250 W). Then, the purple solid (ZIF-67) was separated by centrifugation and washed with DMF three times and dried at 100°C for 24 hours.

*2.4. Preparation and Modification of Electrode.* Prior to the modification, the electrode surface was cleaned with ethanol and polished with alumina (0.05 $\mu$m). A 1 $mg.L^{-1}$ suspension of ZIF-67/rGO in water was prepared by dispersing 10 mg ZIF-67/rGO into 10 mL of distilled water under ultrasonic condition for 4 hours. The modified electrode was obtained by drop-cast 5 $\mu$L of ZIF-67/rGO suspension on the surface of GCE and then dried at ambient temperature. The rGO

or ZIF-67 modified electrode was fabricated in a similar manner by replacing ZIF-67/rGO suspension with ZIF-67 or rGO one.

The samples of tomato and chili sauces were purchased in local area. 15.0 grams of sample was dispersed in 30.0 mL distilled water under ultrasonic stirring within 4 hours and filtered. The RhB concentration in the filtrate was then determined by the proposed method under optimized conditions.

## 3. Results and Discussion

*3.1. Characterization of ZIF-67/rGO Composite.* XRD patterns of reduced graphene oxide (rGO), ZIF-67, and ZIF-67/rGO composite were obtained and compared (Figure 1). Figure 1(a) presents a weak and broad reflection peak at *ac.* 26° corresponding to the relative short-range order structures in disordered stacked rGO [14], which indicates the successful reduction of graphene oxide. The XRD pattern in Figure 1(b) exhibits the characteristic peaks of ZIF-67 corresponding to planes (011), (002), (112), (022), (013), (222), (114), (223), (244), (134), (044), (334), and (235) according to CCDC671073 database. The formation of ZIF-67/rGO composite is confirmed with the appearance of the characteristic peaks of ZIF-67 in the XRD pattern but in lower intensity. The characteristic peaks of rGO at 26° are not observed due to the overlap of ZIF-67 diffractions.

The morphology of the obtained materials was observed by TEM and SEM images. The TEM image of rGO shows a stacked and crumpled morphology, revealing deformation because of the exfoliation and restacking process [15] (Figure 2(a)). The ZIF-67 crystal particles aggregated and were in uniform polyhedral morphology with the size of $140 \pm 5.6$ nm (counted for 50 particles) (Figure 2(b)). The TEM image of ZIF-67/rGO composite shows that the ZIF-67 particles with an average size of 50-70 nm dispersed well on the rGO sheet (Figure 2(c)). The formation of composite material in this experimental condition can be explained when considering the possible interactions between the reactants. Upon adding $Co^{2+}$ to rGO suspension, there may be an interaction between $Co^{2+}$ with oxygen-containing functional group in rGO, although this interaction can be weak. Therefore, as 2-methylimidazole is introduced into the mixture, its bonding to $Co^{2+}$, which is stronger than its competence mentioned above, is formed to generate ZIF-67 as particles of around 10-20 nm dispersing on the rGO matrix as shown in Figure 2(c). The synthesis of ZIF-67 on rGO matrix limits the possibility of ZIF-67 crystals growth. Consequently, its size is significantly smaller compared with that of ZIF-67 synthesized separately as shown in Figure 2(c).

The formation of ZIF-67, rGO, and ZIF-67/rGO composite is also confirmed by the FT-IR spectra (Figure 3). The position of characteristic absorption bands of ZIF-67 synthesized in this study is in good agreement with those reported previously [16]. The absorption band centered at 3441 $cm^{-1}$ is assigned to the stretching of OH in water adsorbed in material. The main absorption peaks from 600-1500 $cm^{-1}$ are assigned to the vibrations of functional groups in

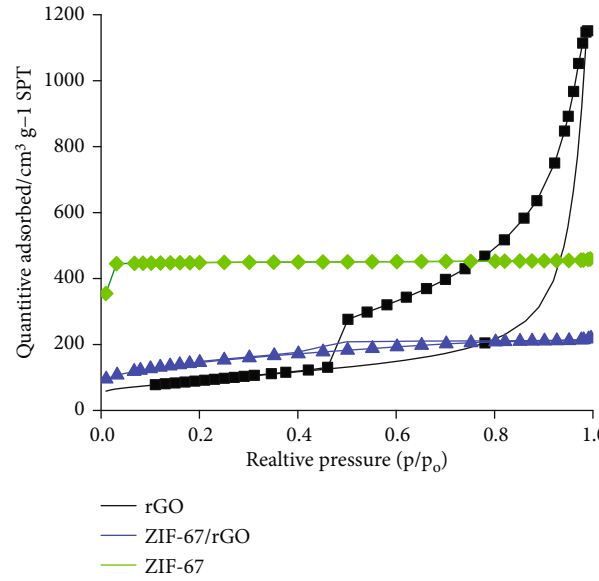


Figure 6: Nitrogen adsorption/desorption isotherms of ZIF-67 (green), rGO (black), and ZIF-67/rGO (blue).

2-methylimidazole, in which the peak at 1578 $cm^{-1}$ can be attributed to the stretching vibration of C=N bond and the peak at 2924 $cm^{-1}$ belongs to the symmetric stretching vibration of $CH_3$ [17]. The absorption band at 1573 $cm^{-1}$ in the FT-IR spectrum of rGO can be attributed to the skeletal vibration of graphene sheets. The vibration of C–O stretching of epoxy group and alkoxy is observed at broad peak from 1220 $cm^{-1}$ to 1067 $cm^{-1}$ due to incomplete reduction of GO [18]. The FT-IR spectrum for ZIF-67/rGO exhibits a combination of infrared peaks of ZIF-67 and rGO indicating that the structures of ZIF-67 and GO are maintained in the composite.

Raman spectroscopy can also be employed to effectively probe the disorder in the carbon structure of the material. In the Raman spectra of rGO and rGO/ZIF-67 (Figure 4), two peaks are clearly visible at 1336 $cm^{-1}$ and 1602 $cm^{-1}$, corresponding to the so-called D and G bands, respectively. It is reported that the D band peak corresponds to the breathing mode of $\kappa$-point phonons of $A_{1g}$ symmetry, and the G band peak represents the first-order scattering of the $E_{2g}$ phonons [19]. The intensity of the D band is related to the size of the in-plane sp2 domains, and the relative intensity ratio ($ID/IG$) is a measure of the extent of disorder [19]. An increase in intensity ratio ($I_D/I_G$) and the higher intensity of D band indicate the presence of more isolated graphene domain in ZIF-67/rGO compared to in rGO. It is found that the intensity ratio of $I_D/I_G$ is 1.02 for rGO and 2.01 for ZIF-67/rGO. The results confirm that the composite consists of rGO and ZIF-67 structures.

The oxidation states of elements were examined by XPS (Figure 5). The XPS survey spectrum presents the existence of Co, O, N, and C in ZIF-67/rGO composite (Figure 5(a)). The C1s spectrum of ZIF-67/rGO (Figure 5(b)) is able to be fitted by three components at 284.59, 285.87, and 288.16 eV, corresponding to carbon in aromatic rings, epoxy C-O-C, and carboxyl COOH groups, respectively [15, 20]. These components indicate that the reduction of graphene

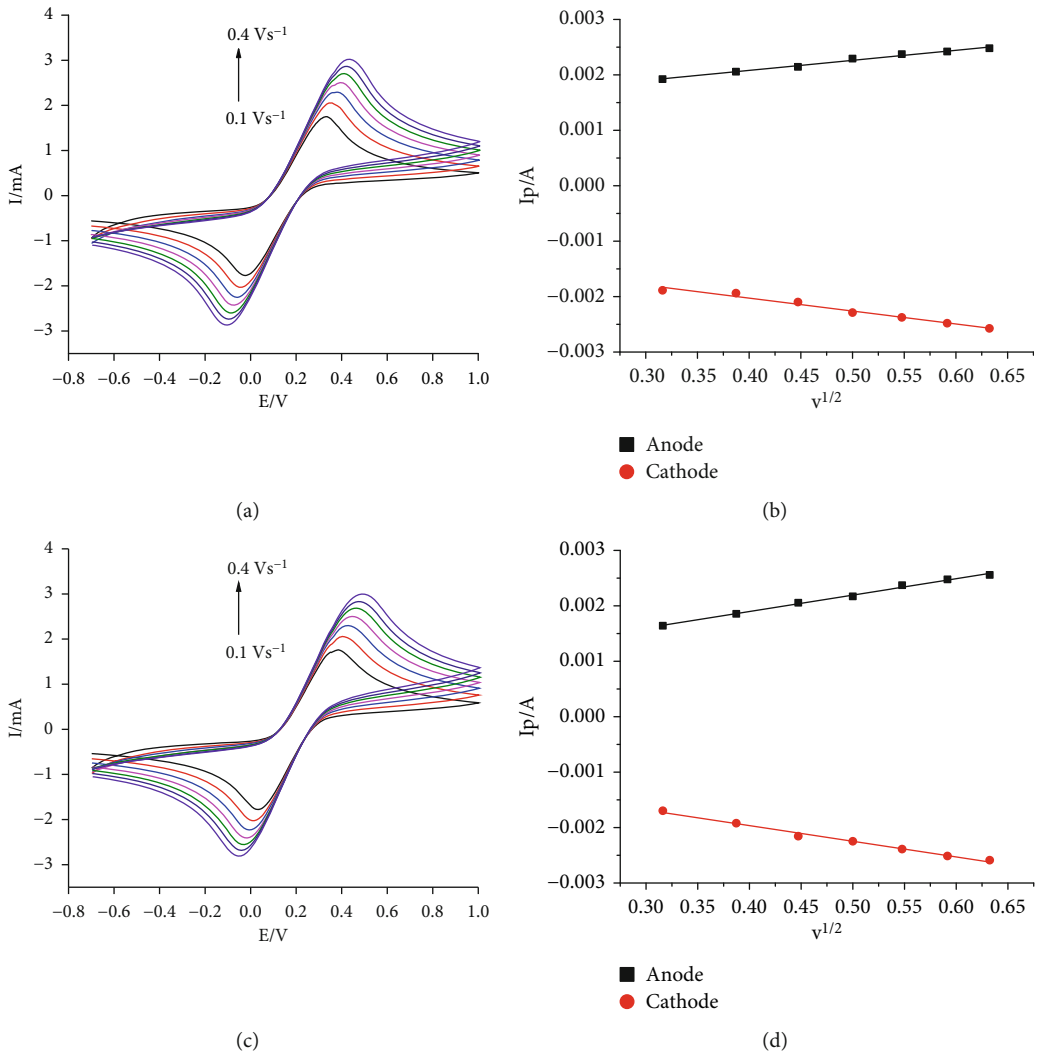


Figure 7: Cyclic voltammograms (CVs) obtained in aqueous solution (0.1 M KCl) containing 1.0 mM $K_3[Fe(CN)_6]$ at designated scan rate (from 0.1 to 0.4 $Vs^{-1}$) at different electrodes (a) bare GCE. (b) The corresponding linear plot of peak current (*Ip*) vs. $v^{1/2}$ and (c) ZIF-67/rGO-GCE. (d) the corresponding linear plot of *Ip* vs. $v^{1/2}$.

oxide is not complete. The N1s XPS spectrum at 400 eV represents a dominant contribution from nitrogen atom in the pyrrolic-N and a shoulder at 398.8 eV, which possibly due to the interaction of N-imidazolate with graphene sheets (Figure 5(c)) [21]. The Co2p spectrum exhibits two main peaks coupled with two satellites, 805.01 eV coupled with 797.7 eV for Co2p1/2 and 785.7 eV coupled with 780.5 eV for Co2p3/2 [22] (Figure 5(d)). The estimation of the oxidation states of Co cations can be done by analyzing the energy gap between the Co2p main peak and the satellite peak. Typically, this energy gap of Co(II) cation is *ca.* 6.0 eV, while that of Co(III) cation is approximately 9-10 eV [23, 24]. In the present case, the energy gap of cobalt cation is 6.27 eV for Co2p1/2 and 5.2 for Co2p3/2. Therefore, Co(II) is the main form in the as-prepared ZIF-67 material.

The textural properties of ZIF-67, rGO, and ZIF-67/rGO were examined via nitrogen adsorption-desorption isotherms (Figure 6). The ZIF-67 material exhibits a typical type-I adsorption isotherm with a high amount of $N_2$ adsorption indicating high porosity. An increase in adsorption volume at a low relative pressure indicates the existence of micropores in all ZIF-67 samples. The isotherm curves of rGO and ZIF-67/rGO belong to typical type IV according to IUPAC classification. The presence of the hysteresis loop at high relative pressure region indicates the existence of mesopore which can be attributed to the void among the primary particles [25, 26]. The specific surface areas of ZIF-67, rGO, and ZIF-67/rGO derived from the BET model are found to be 1330 $m^2.g^{-1}$, 200 $m^2.g^{-1}$, and 498 $m^2.g^{-1}$, respectively. The surface area ZIF-67/rGO sample in this study is higher than that of rGO based materials reported previously [27, 28].

### 3.2. Voltammetric Determination of Rh-B Using ZIF-67/rGO Modified Electrode

*3.2.1. The Electroactive Surface Area of ZIF-67/rGO-GCE.* The electrochemical behavior of different electrodes was characterized via cyclic voltammetry (CV) experiments on $K_3[Fe(CN)_6]$ solution. Figures 7(a) and 7(c) present the

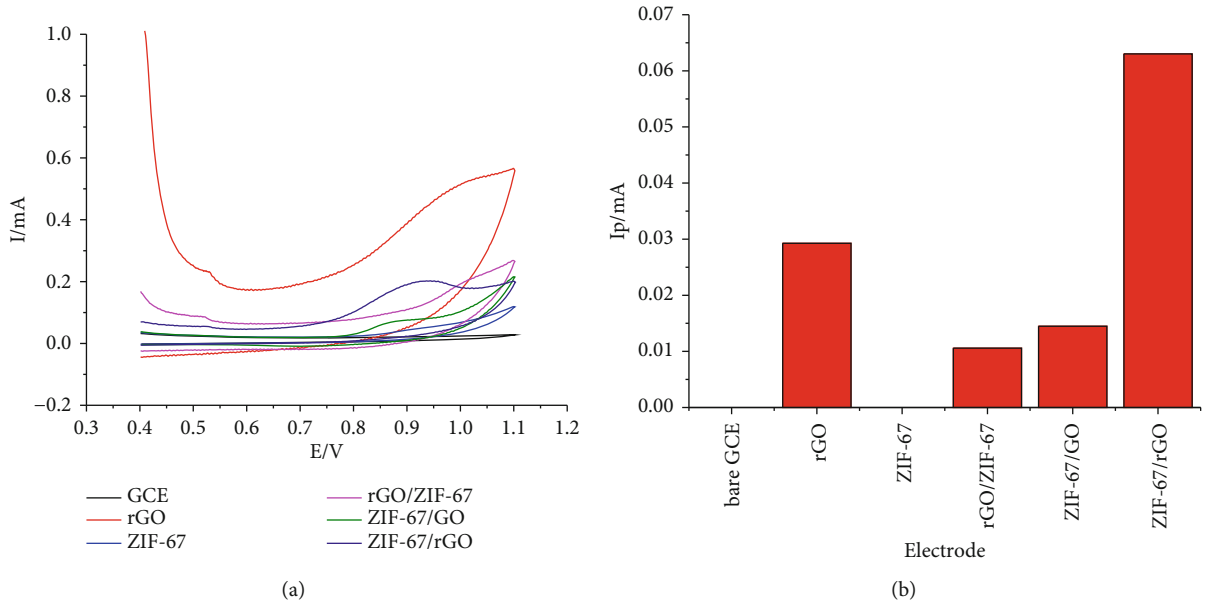


Figure 8: (a) CVs obtained in aqueous solution containing 24 mg/L RhB (0.1 M BR-BS pH 6) and (b) the corresponding anodic peak currents at different electrodes.

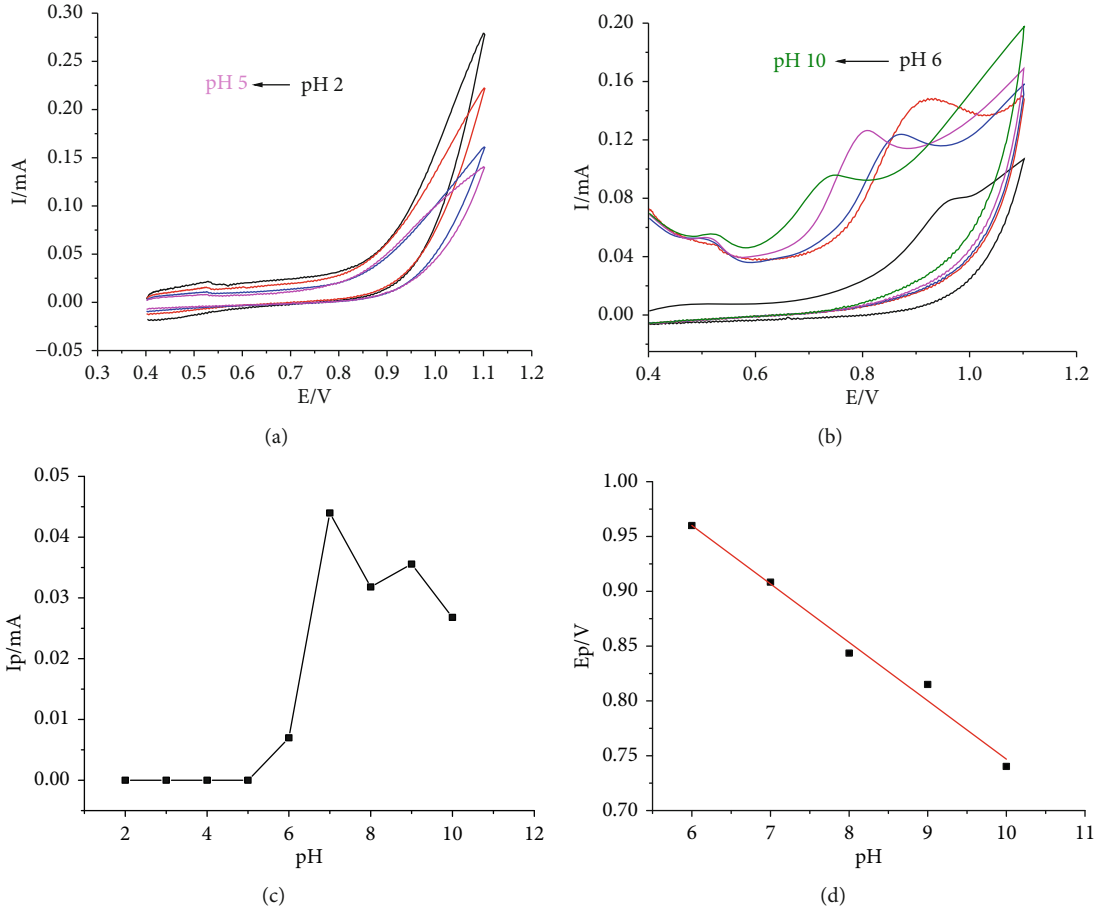


Figure 9: (a) Cyclic voltammograms (CV) obtaining with ZIF-67/rGO-GCE in aqueous solution containing 24 mg/L RhB at pH = 2 – 5. (b) At pH = 6 – 10. (c) The dependence of pH on the anodic peak current (*Ip*). (d) The linear plot of the anodic peak potential (*Ep*) *vs.* pH.

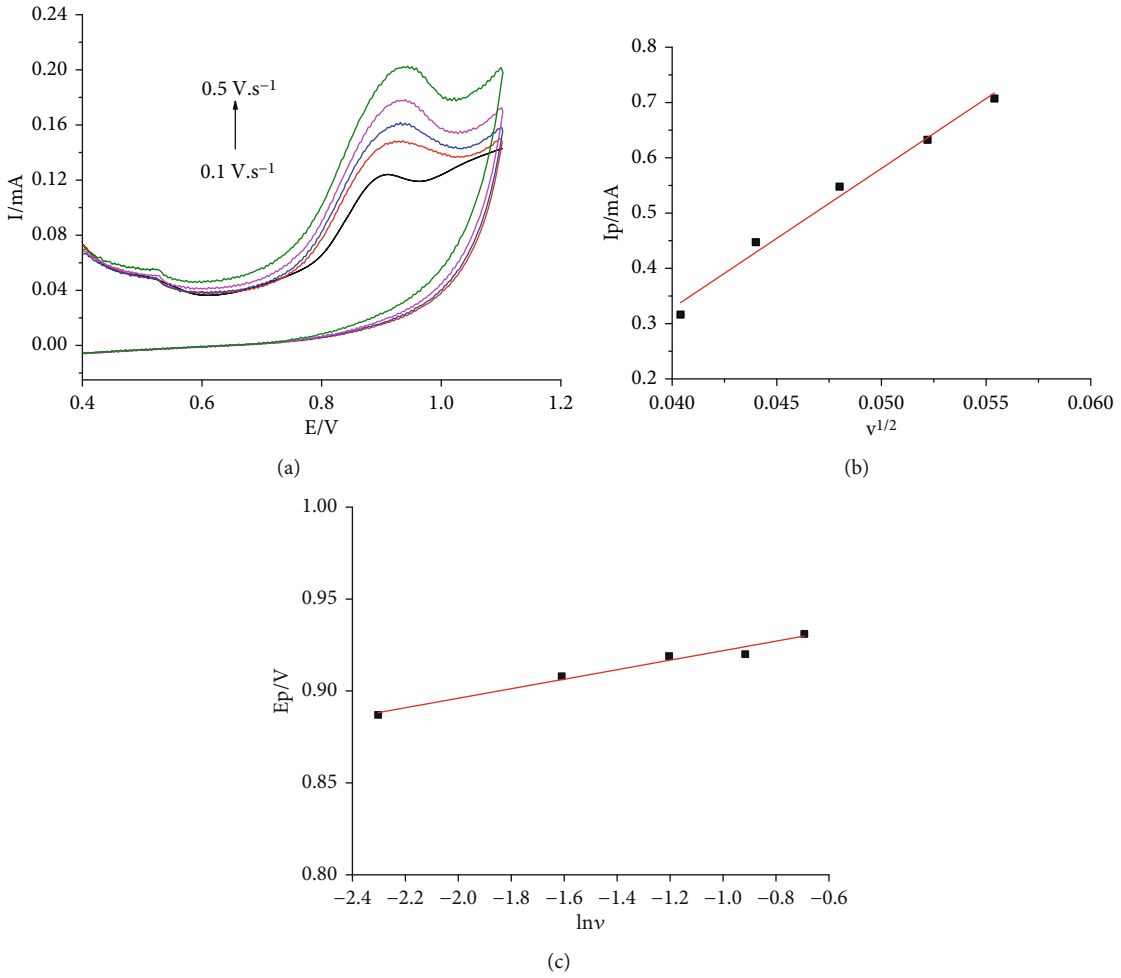


Figure 10: (a) CVs obtained with ZIF-67/rGO-GCE in aqueous solution (0.1 M BR-BS pH 7) containing 24 mg/L RhB at designated scan rates. (b) The plot of *Ipvs.* $v^{1/2}$. (c) The linear plot *Epvs* ln*v*.

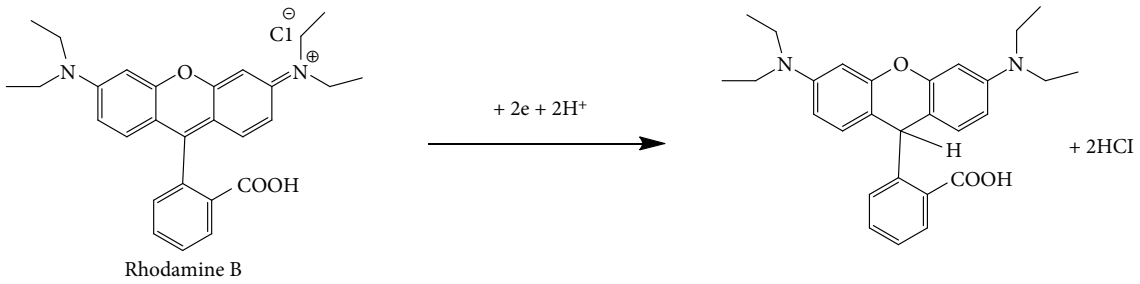


Scheme 1: Oxidation mechanism of RhB.

CVs using bare GCE and ZIF67/rGO/GCE in 1.0 mM $[Fe(CN)_6]^{3-}$ solution (0.1 M KCl). For a reversible process, the anodic peak current (*I*pa) is proportional to the square root of scan rates (*v*1/2) as describe in Randles-Sevcik formula:

$$Ipa = 2.69x10^5 n^{3/2} AD^{1/2} C0v^{1/2} \quad (1)$$

where *I*pa is the peak current (anodic peak current), *n* is the number of electrons transferred (*n* = 1 in the $[Fe(CN)_6]^{3-/4-}$ redox system), *A* is the surface area of electrode ($cm^2$), *C*0 is the concentration of $[Fe(CN)_6]^{3-}$, *D*0 is the diffusion coefficient of the $[Fe(CN)_6]^{3-/4-}$ (*C*o = 1 mM; 6.7 × 10 − 6 cm2 s − 1 [29]), and *v* is the scan rate ($V.s^{-1}$).

Therefore, from the linear plot of the *I*pa versus $v^{1/2}$ (Figures 7(b) and 7(d)), the value of *A* is found to be 0.070 $cm^2$ for bare GCE and 0.117 $cm^2$ for ZIF-67/rGO-GCE indicating that the effective electroactive surface area of the modified electrodes is improved significantly.

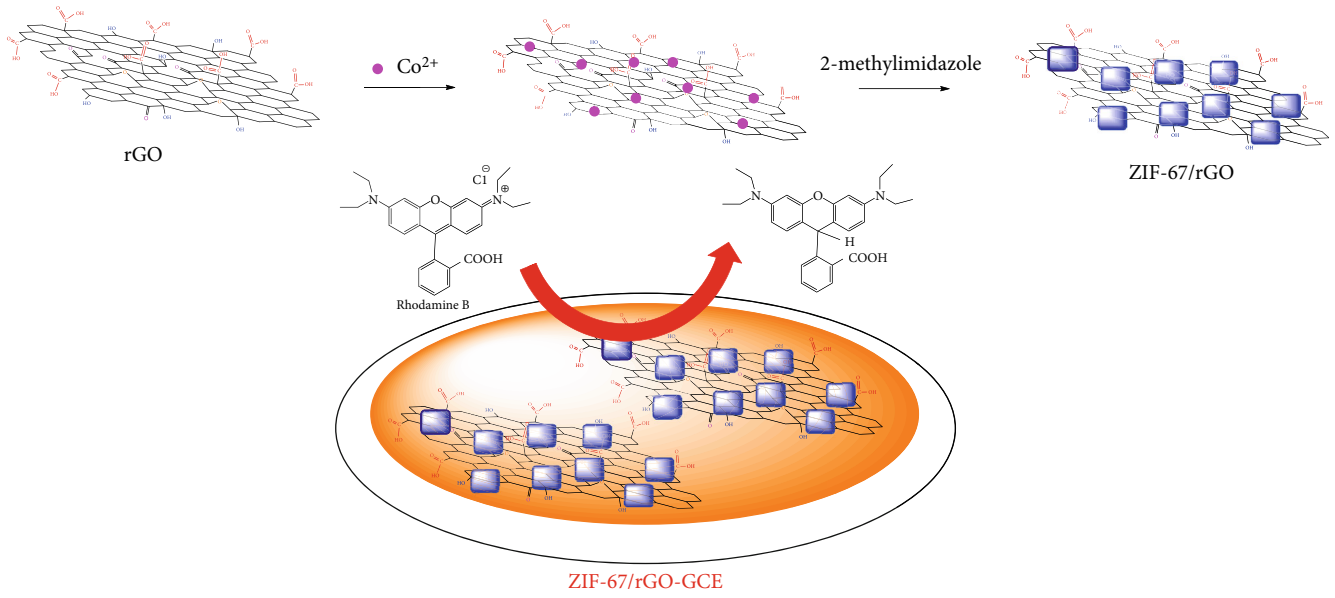


Scheme 2: The proposed mechanism of electrode process for RhB oxidation.

*3.2.2. Cyclic Voltammetry Behavior of RhB at ZIF-67/rGO/GCE*

*(1) Cyclic Voltammetry Behavior*. Figure 8(a) presents the CVs of RhB at bare GCE, ZIF-67/GCE, rGO/GCE, and ZIF-67/rGO-GCE. It is clear that there is no obvious redox peak on the CVs with the use of bare GCE and ZIF-67/GCE. When rGO/GCE was used, on the scan toward positive potential, the rise of oxidation current at 0.92 V indicating an oxidation process of RhB at the electrode surface. No reduction process can be observed on the reversed scan suggesting that this is an irreversible process. However, the CV behavior on ZIF-67/rGO-GCE assembles that on rGO/GCE, except the fact that this electrode significantly enhances not only the shape of the oxidation peak but also the peak current at 0.92 V. It is found that the peak current magnitude is 2.2 times higher compared with rGO/GCE (Figure 8(b)). The ZIF-67/rGO-GCE exhibits good electroactivity toward the oxidation of RhB probably due to the synergistic effect of high electrical conductivity of rGO [30] and excellent textural properties of ZIF-67, including large surface area, abundant number of adsorptive sites, and large volume of porosity.

*(2) Effect of pH*. Figure 9 presents the effect of pH on electrochemical responses of CV. At solution pH lower than 5, the oxidation peak cannot be observed (Figure 9(a)). However, the peak becomes more apparent at pH> 6 and the peak current magnitude reaches a maximum value at pH 7 (Figures 9(b) and 9(c)). Hence, pH = 7 was selected for further experiments. Furthermore, upon increasing pH from 6 to 10, the peak potential shifts to more negative value from 0.96 V to 0.74 V indicating that the protons are involved in the RhB oxidation at electrode. The relationship between pH of solution and oxidation peak potential is plotted as in Figure 9(d) illustrating a linear correlation.

Table 1: Tolerance limit of interfering species at 5.7 $\mu g.L^{-1}$ RhB.

| Interferent | Concentration interferent (mg/L) | Concentration ratio of Interferent/RhB | RSD (%) |
|---|---|---|---|
| Saccharine | 570 | 100 | 4.2 |
| Glucose | 342 | 60 | 5 |
| Sodium benzoate | 285 | 50 | 4.9 |
| Saccharine | 285 | 50 | 4.2 |
| $K_2CO_3$ | 583 | >100 | <5 |
| $Na_2SO_4$ | 285 | 50 | 4.3 |
| $Ca(H_2PO_4)_2$ | 580 | >100 | <5 |
| NaCl | 595 | >100 | <5 |

The linear regression equation of *Ep* against pH is expressed as follows:

$$Ep = (1.27 \pm 0.03) + (-0.053 \pm 0.003)pH \quad r = 0.993 \quad (2)$$

The value of 0.053 is close to the theoretical Nestian value of 0.0592 (Figure 9(d)) implying that the oxidation reaction of RhB at electrode involves an equal number of electrons and protons.

*(3) Effect of Scan Rate*. Effect of scan rate on electrochemical signals also provides the information on oxidation mechanism (Figure 10). Upon increasing scan rates, the cathodic peak current magnitude grows along with the shift of peak potential to more positive value as shown in Figure 10(a) implying a nondiffusion controlled process.

In order to confirm whether the electrooxidation reaction is diffusion controlled or adsorption controlled, the

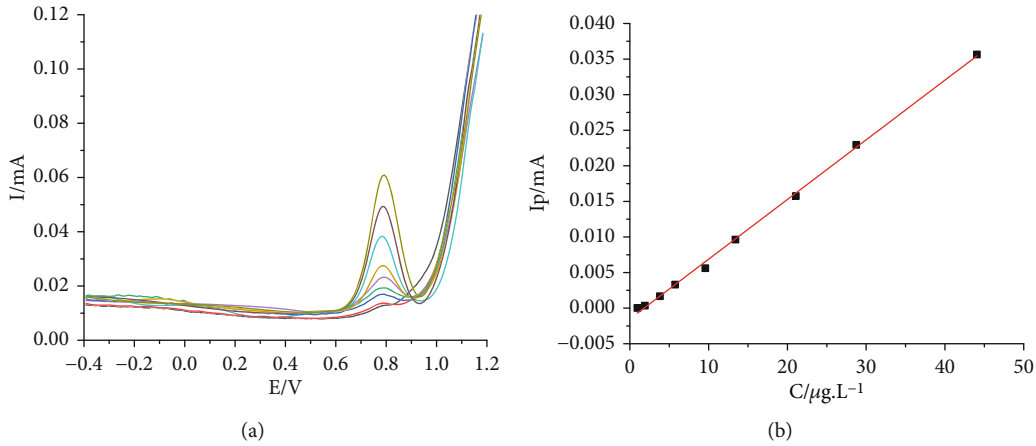


FIGURE 11: (a) DPV curves of different concentration of RhB at ZIF-67/rGO modified electrode in 0.1 M BR-BS pH 7. (b) A linear plot of *I*pa *vs.* RhB concentration.

dependence between $Ip$ and $v^{1/2}$ was plotted (Figure 10(b)). The linear regression equation of $Ip$ vs $v^{1/2}$ is derived as follows:

$$Ip = (0.039 \pm 0.008)\, v^{1/2} + (0.027 \pm 0.0045), r = 0.993 \quad (3)$$

The plot of $Ip$ vs. square root of the scan rate is highly linear ($r = 0.993$). The value in bracket presents the confidence interval of 95%. With a confidence interval of 95%, the intercept varies from 0.023 to 0.032 which means that the oxidation of RhB at the modified electrode is an adsorption controlled process [14, 31].

The dependence of anodic peak potential ($Ep$) on the scan rate also provides another insight into the mechanism of the process. The number of electrons transferred during the oxidation process can be determined via the relation of peak potential ($Ep$) and natural logarithm of scan rate expressed by Laviron equation: [32].

$$E_p = E^0 - \frac{RT}{(1-\alpha)nF} \ln \frac{RTK_s}{(1-\alpha)nF} + \frac{RT}{(1-\alpha)nF} \ln v \quad (4)$$

where $E0$ is the formal redox potential, $ks$ is the apparent electron-transfer rate constant, $\alpha$ is the charge transfer coefficient, $n$ is the number of electrons transferred, $v$ is the scan rate ($V.s^{-1}$), and $T = 298$ K, $R = 8.314$ J mol K − 1, and $F = 96480$ C mol − 1.

From the plot (Figure 10(c)), the linear regression equation of $Ep$ vs. $lnv$ can be written as follow:

$$Ep, RhB = (0.112 \pm 0.004) + (0.026 \pm 0.003) \ln (v) \quad r = 0.984 \quad (5)$$

The value of $n(1-\alpha)$ obtained from the slope of the linear regression line of Eq. (6) is found as 0.99. The value of $\alpha$ is assumed to be 0.5, which is commonly used for a totally irreversible system [33]. Therefore, the number of electrons transferred ($n$) in the electro-oxidation of RhB is 1.98, which implies that the oxidation mechanisms for RhB can involve two electrons and two protons.

The oxidation mechanism of RhB oxidation on the electrode surface can be illustrated in Scheme 1.

The enhancement of RhB oxidation on ZIF-67/rGO/GCE can be explained by the improvement of RhB absorption on this electrode due to the contribution of various intermolecular interactions between RhB and each individual component of the electrode. The interaction can be electrostatic interaction between ionic RhB with charged ZIF-67/rGO surface, depending on pH, or $\pi$–$\pi$ stacking interactions between 2-methylimidazole ligand of ZIF-67 and the $\pi$-electron of benzene ring in RhB moiety, or complexation interaction between Co(II) and carboxyl group (Scheme 2).

*3.2.3. Quantitative Determination of RhB Using Differential Pulse Voltammetry Method (DPV).* Differential pulse voltammetry method, which is more sensitive than the CV approach, using a ZIF67/rGO/GCE was investigated to quantify the RhB content in real samples, normally at low concentration. By using a solution containing 21.1 $\mu$g/L RhB, the operational parameters were optimized as follows: accumulation potential: -0.2 V; accumulation time: 20s; pulse altitude: 0.06 V; rating potential: 0.008 V (Figure S1-4).

*(1) Interference, Reproducibility, Repeatability, Linear Range and Limit of Detection*. Relative standard deviation (RSD) is applied to estimate the effect of some potential interfering species on the detection of RhB in which the $RSD = (Io - I)/Io$ where $Io$ is peak current measured without and with interference. The tolerance limit is defined as the maximum concentration of the interferent that leads to a RSD of over ±5%. This value of some possible inorganic and organic substances in the use of 5.7 $\mu g.L^{-1}$ RhB is given in Table 1. For inorganic salts, except for $Na_2SO_4$, tested at 50-fold excess, all other inorganic substances at 100-fold excess show no interference effect on the detection of RhB. Similarly, saccharine (at 100-fold excess), glucose (60-fold excess), sodium benzoate, and saccharine (50-fold excess) do not interfere the signal of RhB.

The reproducibility was investigated with nine individual ZIF-67/rGO-GCEs in the detection of 5.7 $\mu$g/L RhB under

Table 2: Comparison of LOD and linear range of the proposed method with the previous methods.

| Methods | Linear range ($\mu$g/L) | LOD ($\mu$g/L) | References |
|---|---|---|---|
| Magnetic solid phase extraction with ionic liquid coated-core shell-magnetic nanoparticles followed by high-performance liquid chromatography | 0.5–150 | 0.08 | [4] |
| Solid phase extraction with Sepab eads SP 70 resin followed by UV-Vis spectrophotometry | 250–3000 | 3.4 | [3] |
| Micelles mediated separation fluorimetric methodology | 0.0467–100 | 0.014 | [1] |
| Cyclodextrin-functionalized nanogold/hollow carbon nanospheres modified electrode, DPV method | 4.79–958.00 | 0.96 | [9] |
| Silica-pillared zirconium phosphate/nafion Composite modified glassy carbon electrode, DPV | 0.005–2.395 | 2.06 | [8] |
| Core-shell structured Cu@carbon sphere nanohybrid modified electrode, DPV | 143.7–1437 | 47.9 | [35] |
| Glassy carbon electrode, DPV | 4.78–956.1 | 2.93 | [36] |
| ZIF-67/rGO modified electrode, DPV | 0.96–44.07 | 1.79 | The present work |

Table 3: Recovery and precision of Rhodamine B in different spiked food samples.

| Sample | RhB added ($\mu$g/mL) | DPV | | HPLC | |
|---|---|---|---|---|---|
| | | RhB found ± SD ($\mu$g/mL) | ReV (%) | RhB found ± SD ($\mu$g/mL) | ReV (%) |
| Tomato sauce #1 | 0 | 0 | 98 | 0 | 99 |
| | 100 | 98.0 ± 0.9 | | 99.2 ± 0.5 | |
| Tomato sauce #2 | 0 | 0 | 96 | 0 | 101 |
| | 100 | 95.9 ± 0.8 | | 101 ± 1 | |
| Chili sauce | 0 | 0 | 103 | 0 | 98 |
| | 100 | 103.0 ± 2.0 | | 98.3 ± 0.2 | |

SD: standard derivation; ReV: recovery.

the optimized conditions. It was found that a good reproducibility with the RSD of the current responses of 7.0% can be obtained. The expectable RSD for nine independent electrodes indicates the good reproducibility of the ZIF-67/rGO-GCE in the present work.

The repeatability of ZIF-67/rGO-GCE for DPV was also studied with the solutions of 5.7; 21.1 and 44.1 $\mu$g/L RhB. The determination of 5.7, 21.1, and 44.1 $\mu$g/L RhB was measured successively for nine times (Figure S5). The obtained RSD for 5.7, 21.1, and 44.1 $\mu$g/L RhB was 6.2, 3.9, and 0.8%, respectively, which are lower than the 1/2 $RSD_{\text{Horwitz predicted}}$ [34]. Such reasonable RSD of successive measurements confirm that the ZIF-67/rGO-GCE is able to be repeatedly used for the determination of RhB in either low concentration range or high concentration range.

Figure 11 presents the DPV curves of different RhB concentration in 0.1 M BR-BS pH 7. As shown in the figure, the linear concentration range of RhB is 0.96–44.07 $\mu$g/L and the regression equation is expressed as follows:

$$Ipa = (-0.0015 \pm 0.0001) + (8.38643 \pm 0.00001)C_{RhB} \quad r = 0.999 \tag{6}$$

The LOD, calculated by 3 $Sy/b$, where Sy is the standard deviation of $y$-residuals and $b$ is the slope of linearity, is found to be 1.79 $\mu g.L^{-1}$.

The detection performance of the ZIF-67/rGO modified electrode in DPV method was compared with the other methods as shown in Table 2. It could be noticed that the linear range and LOD of RhB at the ZIF-67/rGO-GCE are lower or comparable with those results reported previously. The ZIF-67/rGO modified electrode presents a lower LOD compared to UV-Vis spectrophotoscopy method with solid phase extraction using Sepab eads SP 70 resin, or voltammetric method using silica-pillared zirconium phosphate/nafion composite modified glassy carbon electrode. Overall, the ZIF-67/rGO composite is proved to be an effective electrode modifier for the detection of RhB in aqueous solution.

*3.2.4. Real Sample Analysis.* In order to assess the application of the proposed method on real samples, two samples of tomato sauce and one of the chili sauce were chosen to use for the spiked experiments in comparison with the results from high-performance liquid chromatography (HPLC). The results are given in Table 3 showing that all samples are free of RhB and the recovery is in the exceptional range of 98–103% with RSD less than 2%. The results obtained by this method are in statistical agreement with those by HPLC method (paired samples $t$-test, $t(2) = 0.99$, $p = 0.427 > \alpha = 0.05$) manifesting that the voltammetric method using ZIF-67/rGO-GCE is satisfactory.

## 4. Conclusions

A novel modified electrode for RhB quantifying was developed based on the composite of ZIF-67 and reduced graphene oxide. Owing to synergetic effects from rGO with good electroconductivity properties and ZIF-67 with excellent textural properties, the use of ZIF-67/rGO modified electrode in DPV technique provides the broad linear response range and low LOD of RhB detection. Furthermore, the ZIF-67/rGO-GCE has good stability and reproducibility making the proposed method a prospective application for the determination of RhB in foodstuffs.

## Data Availability

The data used to support the findings of this study are available from the corresponding author upon request.

## Conflicts of Interest

The authors declare that they have no conflicts of interest.

## Acknowledgments

This research is funded by Vietnam National Foundation for Science and Technology Development (NAFOSTED) under grant number 104.06-2018.15.

## Supplementary Materials

Figure S1: (a) DPV curves of 21.1 $\mu$g/L RhB in 0.1 M BR-BS pH 7 and (b) anodic peak current (Ip) at different accumulation potentials. Figure S2: (a) DPV curves of 21.1 $\mu$g/L RhB in 0.1 M BR-BS pH 7 and (b) anodic peak current (Ip) at different accumulation times. Figure S3: (a) DPV curves of 21.1 $\mu$g/L RhB in 0.1 M BR-BS pH 7 and (b) anodic peak current (Ip) at different pulse amplitudes. Figure S4: (a) DPV curves of 21.1 $\mu$g/L RhB in 0.1 M BR-BS pH 7 and (b) anodic peak current (Ip) at different rating potentials. Figure S5: DPV curves measured successively for nine times at 5.7, 21.1, and 44.1 $\mu$g/L RhB. *(Supplementary Materials)*

## References

[1] M. Alesso, G. Bondioli, M. C. Talío, M. O. Luconi, and L. P. Fernández, "Micelles mediated separation fluorimetric methodology for rhodamine B determination in condiments, snacks and candies," *Food Chemistry*, vol. 134, no. 1, pp. 513–517, 2012.

[2] N. Pourreza, S. Rastegarzadeh, and A. Larki, "Micelle-mediated cloud point extraction and spectrophotometric determination of rhodamine B using triton X-100," *Talanta*, vol. 77, no. 2, pp. 733–736, 2008.

[3] M. Soylak, Y. E. Unsal, E. Yilmaz, and M. Tuzen, "Determination of rhodamine B in soft drink, waste water and lipstick samples after solid phase extraction," *Food and Chemical Toxicology*, vol. 49, no. 8, pp. 1796–1799, 2011.

[4] J. Chen and X. Zhu, "Magnetic solid phase extraction using ionic liquid-coated core-shell magnetic nanoparticles followed by high-performance liquid chromatography for determination of rhodamine B in food samples," *Food Chemistry*, vol. 200, pp. 10–15, 2016.

[5] C. Franke, H. Westerholm, and R. Niessner, "Solid-phase extraction (SPE) of the fluorescence tracers uranine and sulphorhodamine B," *Science*, vol. 31, no. 10, pp. 2633–2637, 1997.

[6] L. Gagliardi, D. De Orsi, G. Cavazzutti, G. Multari, and D. Tonelli, "HPLC determination of rhodamine B (C.I. 45170) in cosmetic products," *Chromatographia*, vol. 43, no. 1–2, pp. 76–78, 1996.

[7] D. Sun and X. Yang, "Rapid determination of toxic rhodamine B in food samples using exfoliated graphene-modified electrode," *Food Analytical Methods*, vol. 10, no. 6, pp. 2046–2052, 2017.

[8] J. Zhang, L. Zhang, W. Wang, and Z. Chen, "Sensitive electrochemical determination of rhodamine B based on a silica-pillared zirconium phosphate/nafion composite modified glassy carbon electrode," *Journal of AOAC International*, vol. 99, no. 3, pp. 760–765, 2016.

[9] Y. Yi, H. Sun, G. Zhu, Z. Zhang, and X. Wu, "Sensitive electrochemical determination of rhodamine B based on cyclodextrin-functionalized nanogold/hollow carbon nanospheres," *Analytical Methods*, vol. 7, no. 12, pp. 4965–4970, 2015.

[10] P. M. Usov, C. McDonnell-Worth, F. Zhou, D. R. MacFarlane, and D. M. D'Alessandro, "The electrochemical transformation of the zeolitic imidazolate framework ZIF-67 in aqueous electrolytes," *Electrochimica Acta*, vol. 153, pp. 433–438, 2015.

[11] L. Yang, L. Yu, M. Sun, and C. Gao, "Zeolitic imidazole framework-67 as an efficient heterogeneous catalyst for the synthesis of ethyl methyl carbonate," *Catalysis Communications*, vol. 54, pp. 86–90, 2014.

[12] W. S. Hummers and R. E. Offeman, "Preparation of Graphitic Oxide," *Journal of the American Chemical Society*, vol. 80, no. 6, article 1339, 1958.

[13] J. Qian, F. Sun, and L. Qin, "Hydrothermal synthesis of zeolitic imidazolate framework-67 (ZIF-67) nanocrystals," *Materials Letters*, vol. 82, no. 55, pp. 220–223, 2012.

[14] J. Soleymani, M. Hasanzadeh, N. Shadjou et al., "A new kinetic-mechanistic approach to elucidate electrooxidation of doxorubicin hydrochloride in unprocessed human fluids using magnetic graphene based nanocomposite modified glassy carbon electrode," *Materials Science and Engineering: C*, vol. 61, pp. 638–650, 2016.

[15] M. Zhang and M. Jia, "High rate capability and long cycle stability Fe3O4–graphene nanocomposite as anode material for lithium ion batteries," *Journal of Alloys and Compounds*, vol. 551, pp. 53–60, 2013.

[16] X. Guo, T. Xing, Y. Lou, and J. Chen, "Controlling ZIF-67 crystals formation through various cobalt sources in aqueous solution," *Journal of Solid State Chemistry*, vol. 235, pp. 107–112, 2016.

[17] Y. Hu, X. Song, Q. Zheng, J. Wang, and J. Pei, "Zeolitic imidazolate framework-67 for shape stabilization and enhanced thermal stability of paraffin-based phase change materials," *RSC Advances*, vol. 9, no. 18, pp. 9962–9967, 2019.

[18] G. Bharath, B. S. Latha, E. H. Alsharaeh, P. Prakash, and N. Ponpandian, "Enhanced hydroxyapatite nanorods formation on graphene oxide nanocomposite as a potential candidate for protein adsorption, pH controlled release and an effective drug delivery platform for cancer therapy," *Analytical Methods*, vol. 9, no. 2, pp. 240–252, 2017.

[19] Y. Y. Wang, Z. . Ni, T. Yu et al., "Raman studies of monolayer graphene: the substrate effect," *Journal of Physical Chemistry C*, vol. 112, no. 29, pp. 10637–10640, 2008.

[20] K. Jayaramulu, J. Masa, O. Tomanec et al., "Nanoporous nitrogen-doped graphene oxide/nickel sulfide composite sheets derived from a metal-organic framework as an efficient electrocatalyst for hydrogen and oxygen evolution," *Advanced Functional Materials*, vol. 27, no. 33, article 1700451, 2017.

[21] J. Qin, S. Wang, and X. Wang, "Visible-light reduction CO2 with dodecahedral zeolitic imidazolate framework ZIF-67 as an efficient co-catalyst," *Applied Catalysis B: Environmental*, vol. 209, pp. 476–482, 2017.

[22] W. Wei, W. Chen, and D. G. Ivey, "Rock salt-spinel structural transformation in anodically electrodeposited Mn-Co-O nanocrystals," *Chemistry of Materials*, vol. 20, no. 5, pp. 1941–1947, 2008.

[23] D. Barreca, C. Massignan, S. Daolio et al., "Composition and microstructure of cobalt oxide thin films obtained from a novel cobalt (II) precursor by chemical vapor deposition," *Chemistry of Materials*, vol. 13, no. 2, pp. 588–593, 2001.

[24] D. G. Castner, P. R. Watson, and I. Y. Chan, "X-ray absorption spectroscopy, X-ray photoelectron spectroscopy, and analytical electron microscopy studies of cobalt catalysts. 1. Characterization of calcined catalysts," *The Journal of Physical Chemistry*, vol. 93, no. 8, pp. 3188–3194, 1989.

[25] Y. Yang, H. Dong, Y. Wang, C. He, Y. Wang, and X. Zhang, "Synthesis of octahedral like Cu-BTC derivatives derived from MOF calcined under different atmosphere for application in CO oxidation," *Journal of Solid State Chemistry*, vol. 258, pp. 582–587, 2018.

[26] X. Zhang, H. Li, X. Lv et al., "Facile synthesis of highly efficient amorphous Mn-MIL-100 catalysts: formation mechanism and structure changes during application in CO oxidation," *Chemistry - A European Journal*, vol. 24, no. 35, pp. 8822–8832, 2018.

[27] Y. Chen, B. Song, X. Tang, L. Lu, and J. Xue, "One-step synthesis of hollow porous Fe3O4 beads–reduced graphene oxide composites with superior battery performance," *Journal of Materials Chemistry*, vol. 22, no. 34, article 17656, 2012.

[28] V. Chandra, J. Park, Y. Chun, J. W. Lee, I. C. Hwang, and K. S. Kim, "Water-Dispersible Magnetite-Reduced Graphene Oxide Composites for Arsenic Removal," *ACS Nano*, vol. 4, no. 7, pp. 3979–3986, 2010.

[29] A. M. Bagoji and S. T. Nandibewoor, "Electrocatalytic redox behavior of graphene films towards acebutolol hydrochloride determination in real samples," *New Journal of Chemistry*, vol. 40, no. 4, pp. 3763–3772, 2016.

[30] V. B. Mohan, R. Brown, K. Jayaraman, and D. Bhattacharyya, "Characterisation of reduced graphene oxide: effects of reduction variables on electrical conductivity," *Materials Science and Engineering: B*, vol. 193, no. C, pp. 49–60, 2015.

[31] A. J. Bard and L. J. Falkner, *Electrochemical methods, fundamentals and applications*, vol. 60, no. 1, 20012ed., Wiley, 2001.

[32] E. Laviron, "General expression of the linear potential sweep voltammogram in the case of diffusionless electrochemical systems," *Journal of Electroanalytical Chemistry*, vol. 101, no. 1, pp. 19–28, 1979.

[33] C. Li, "Electrochemical determination of dipyridamole at a carbon paste electrode using cetyltrimethyl ammonium bromide as enhancing element," *Colloids and Surfaces B: Biointerfaces*, vol. 55, no. 1, pp. 77–83, 2007.

[34] I. Taverniers, M. de Loose, and E. van Bockstaele, "Trends in quality in the analytical laboratory. II. Analytical method validation and quality assurance," *TrAC Trends in Analytical Chemistry*, vol. 23, no. 8, pp. 535–552, 2004.

[35] J. Sun, T. Gan, Y. Li, Z. Shi, and Y. Liu, "Rapid and sensitive strategy for Rhodamine B detection using a novel electrochemical platform based on core-shell structured Cu@carbon sphere nanohybrid," *Journal of Electroanalytical Chemistry*, vol. 724, pp. 87–94, 2014.

[36] L. Yu, Y. Mao, and L. Qu, "Simple voltammetric determination of rhodamine B by using the glassy carbon electrode in fruit juice and preserved fruit," *Food Analytical Methods*, vol. 6, no. 6, pp. 1665–1670, 2013.